INTEGRATED
ENGINEERING SOFTWARE

www.integratedsoft.com

Beam Spot Size as a Function of Excitation Levels of Magnetic Quadrupoles

Content

Executive Summary

This paper will present an overview of the focusing properties of magnetic quadrupoles and show how beam spot size can be determined using arc segment emitters. We will also show how parametric variation of the excitation current can be used to determine the optimum level for minimum spot size at points along the beam axis.

Characteristics of Magnetic Quadrupoles

The picture at right shows a 3D model of an electromagnetic quadrupole. This model (and all models that will be presented in this paper) was created in **LORENTZ** which is CAE beam analysis software package from **INTEGRATED Engineering Software**.

The quadrupole consists of alternating north and south poles attached to a toroidal yoke. The yoke provides a low reluctance path to complete the magnetic circuit.

Current carrying coils are wound around each pole to provide the magnetomotive force that creates the fields in the air gap of the quadrupole. In our models, the **Z axis** will be used as the axis of the quadrupole, and we will simulate charged particles launched in the **Z** direction.

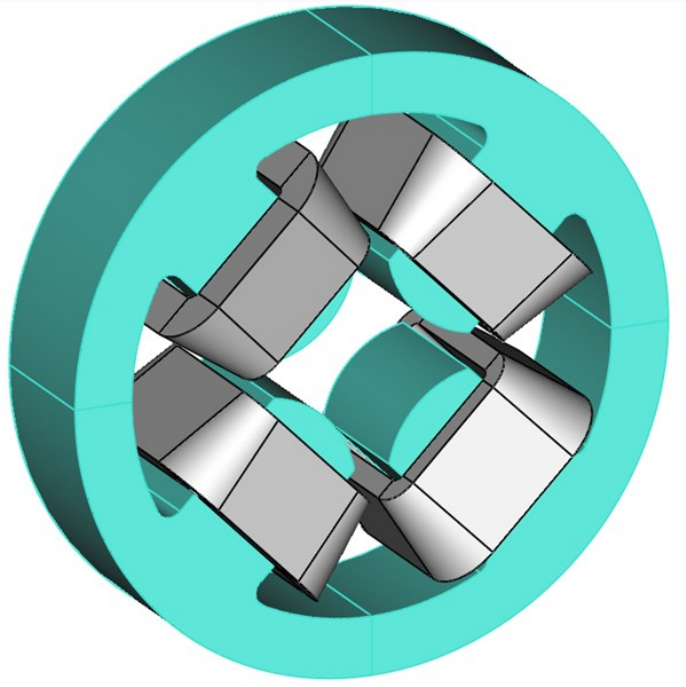

By using **anti-periodic modelling**, it is possible to obtain the complete field solution with only one quarter of the full model geometry. This of course dramatically reduces solution time, and as a side benefit allows better visualization of field results and trajectory simulations.

The picture at right shows the single pole required for the anti-periodic model. Here the remaining coil has been hidden, and the pole has been made semi-transparent so that the contour lines of a vector potential plot can be seen. An arrow plot has been added to show the direction of the magnetic field vectors.

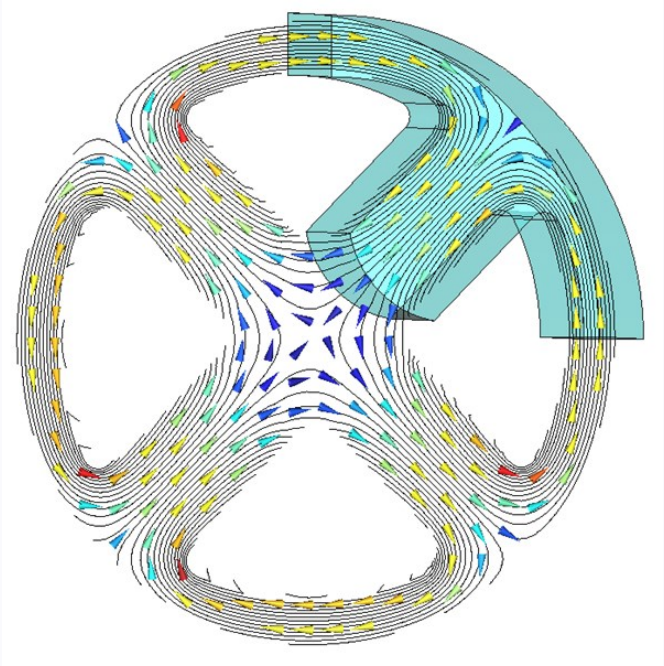

The poles are arranged so that opposite poles produce opposing fields, and as a result there is a complete cancellation of the field along the central axis of the quadrupole. This pole arrangement also creates linear gradients of the field components which we will illustrate using contour plots.

The first contour plot shows the variation of the **X** component of the **B** field in the **X=0** plane. In the middle of the quadrupole there is a linear variation as a function of the **Y** displacement from the central axis. For our magnet model, maximum excitation will produce a negative gradient of the **X** component of **-0.67 T/m**.

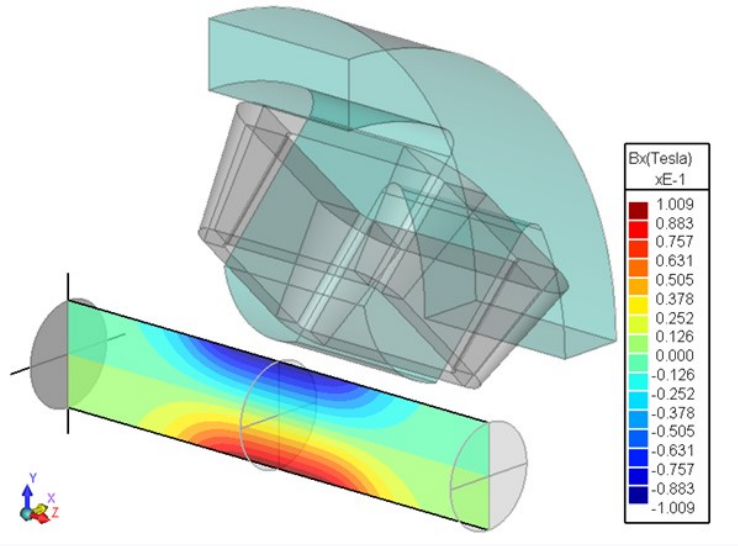

The next plot shows the **Y** component in the **Y=0** plane. In this case the **Y** component varies according to the **X** displacement from the axis again with a negative gradient of -**0.67 T/m**.

The contour plots also show the fringing effects of the **B** field. The fields are maximum in the middle of quadrupole and taper off as a function of the **Z** displacement in either direction.

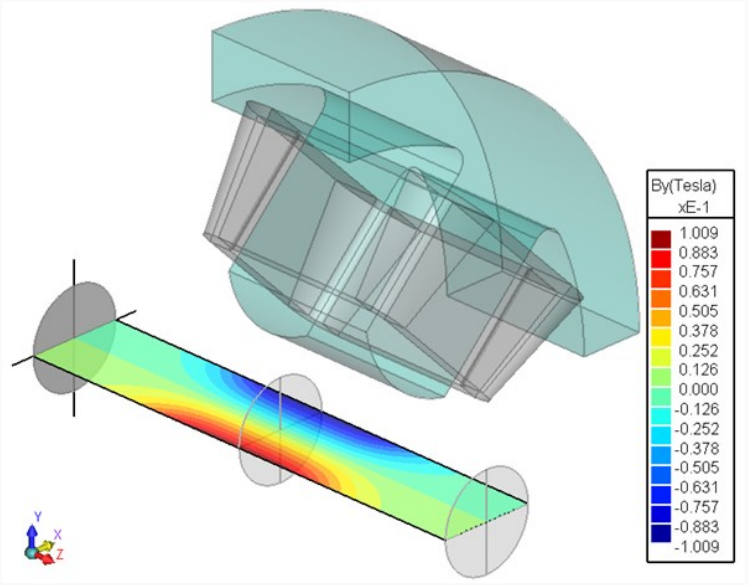

The gradient field variations produce both a desirable focusing effect and an unavoidable defocusing effect depending on ray displacement from the central axis.

The blue trajectories shown at right are the result of positive particles launched in the **Z** direction from points along the **Y** axis. The direction of the Lorentz forces on these particles produces a focusing effect.

If the same particles are launched from points along the **X** axis, the result will be defocusing as shown by the red trajectories.

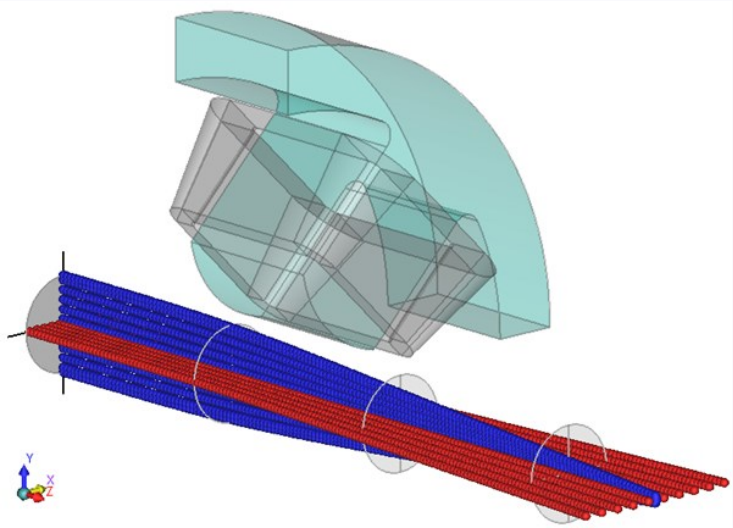

The defocusing can be corrected by adding a second quadrupole with opposite polarity to the first as shown in the picture at right.

It might seem that this would be self-defeating since the second quadrupole will have a defocusing effect on the rays that were focused by the first quadrupole. However, when these rays enter the second quadrupole they will be much closer to the central axis and will experience lower fields as a result.

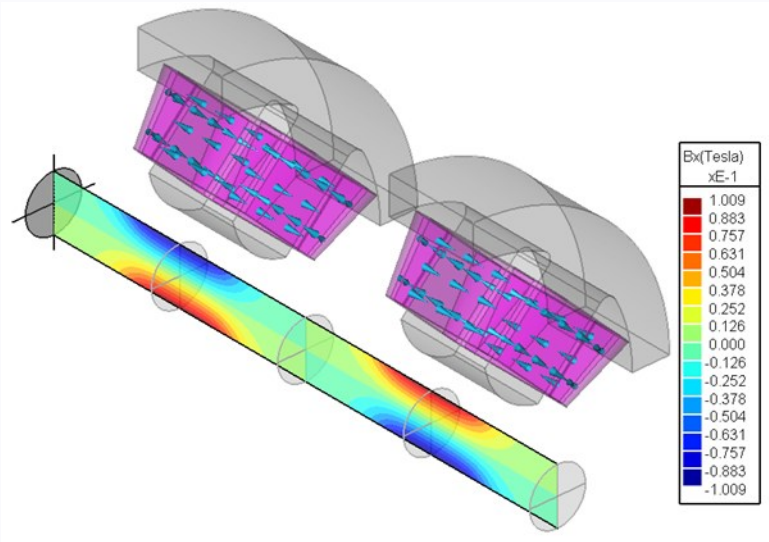

Conversely, the defocused rays will be further from the central axis when they enter the second quadrupole and will therefore experience greater fields.

The net effects are shown at right. The second quadrupole reverses the defocusing of the red rays, but at a cost of pushing the focal point of the blue rays further along the **Z** axis.

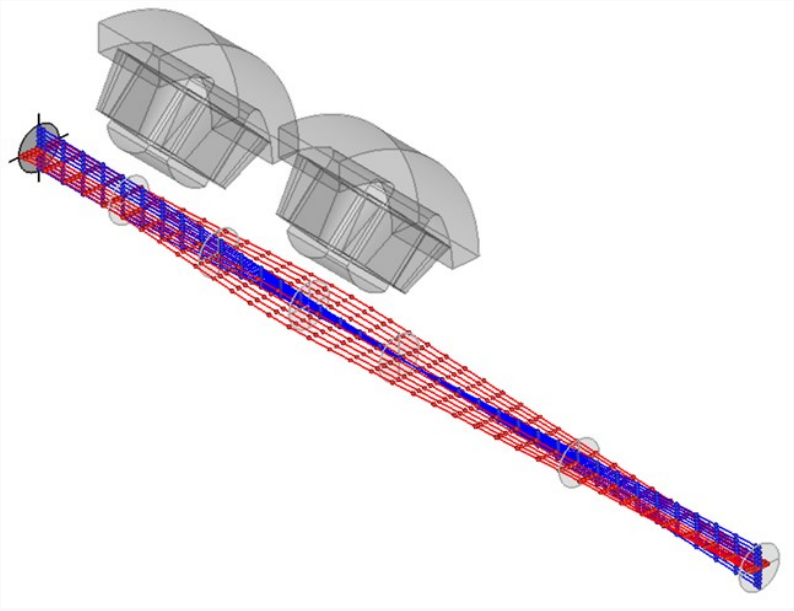

Note that the blue rays diverge past their focal point. Also, for the trajectory simulation limits set in the example above, the red rays have not completely converged to a focus by the time the last simulation time step is reached. The simulation time can of course be increased to determine the focal point of the red rays, but it is important to note that it is impossible to obtain a simultaneous focus of both the red and blue rays.

Magnet and Beam Characteristics

Our simulation model consists of two quadrupoles spaced **1 meter** apart with each having a length of **0.5 meter**. The distance between opposite pole tips is **44.89 cm**, and the diameter of the emitter surface is **30 cm**.

At maximum excitation the coil windings will carry **13,466 Amp*Turns** which for our model corresponds to a current density of **341,500 Amp/m^2** (or **220.32 Amp/in^2**).

We will study the trajectories for beams of **Cs+** ions launched parallel to the central axis with energies of **300 keV**.

Beam Envelope and Spot Size

The trajectory examples we have shown so far have all been launched from segments aligned with the **X** or **Y** axes. While this approach is helpful in understanding the nature of the focusing/defocusing fields, it provides little insight into the shape of beams composed of multiple rays distributed over a larger cross section area.

If we assume that the rays entering the quadrupole are uniformly distributed over a circular surface, then launching trajectories from the circular arcs that form the perimeter of the surface will give an excellent visualization of the beam envelope. This is shown in the picture below.

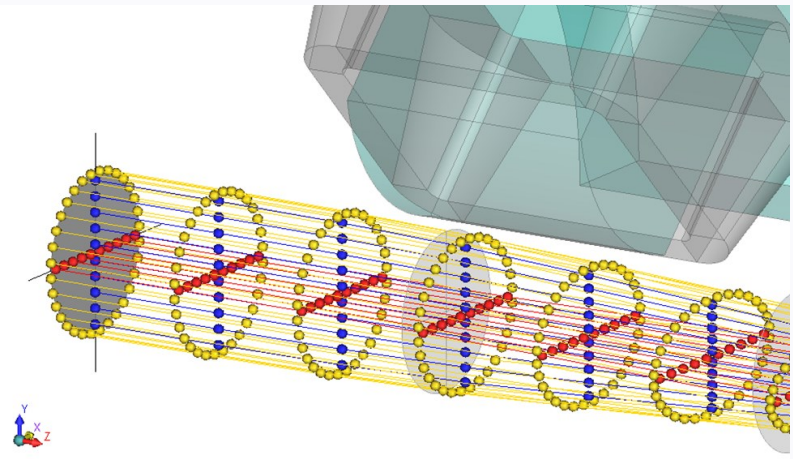

The rays launched from the circular arcs are shown in yellow. It is clear that the effects of the gradient fields result in the distortion of the initially circular beam into elliptical cross sections. We've included the original blue and red rays shown in previous examples, as they provide an indication of the major and minor axes of the ellipses.

When a charged particle beam passes through a device, the size and shape of the beam vary at any given distance along the axis. The smallest diameter of a circle around the beam axis that covers all the beam is termed the **Spot Size**. For points where the beam cross section is circular, the spot size is equal to the diameter of the circle. For points where the beam cross section is elliptical, the spot size will correspond to the major axis of the ellipse. In the **LORENTZ** program, the spot size can also be calculated to include a certain percentage of the beam so that a few stray rays will not have a large effect.

Limitations of the Beam Envelope Approach

Launching rays from the perimeter of an emitter surface provides excellent visualization of the beam envelope and is computationally faster than launching a larger number of rays from points on the emitter surface. However, it must be used with caution since it cannot account for beam spread due to space charge effects.

Spot Size Variation along Beam Axis at Maximum Excitation

Previously we noted that the quadrupole pair would create two separate focal points, and that it is not possible to achieve a single focal point. However, there will be a point along the beam axis for which the spot size of the beam cross section reaches a minimum as we will show in this section.

The picture below shows a circular beam entering the quadrupole system where it is distorted by the combined focusing and defocusing effects. In the picture a rectangle indicates the location where the beam spot size is minimum.

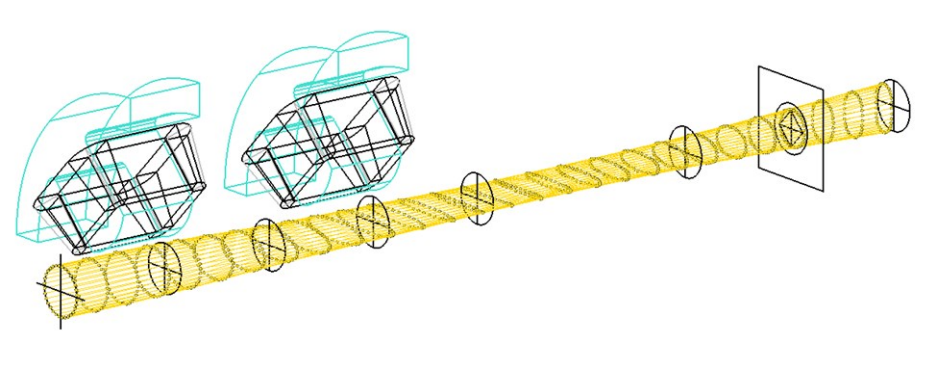

In this example the coil currents are at maximum. Note the complete flattening of the beam that occurs just beyond the second quadrupole; this indicates the first focal point. Note also that the minimum spot size occurs beyond the first focal point.

The picture at right shows a close-up of the region near the minimum spot size. Note that the beam cross section is stretched in the **X** direction before the minimum, and in the **Y** direction past the minimum. At the point where the spot size reaches its minimum the beam cross section is circular.	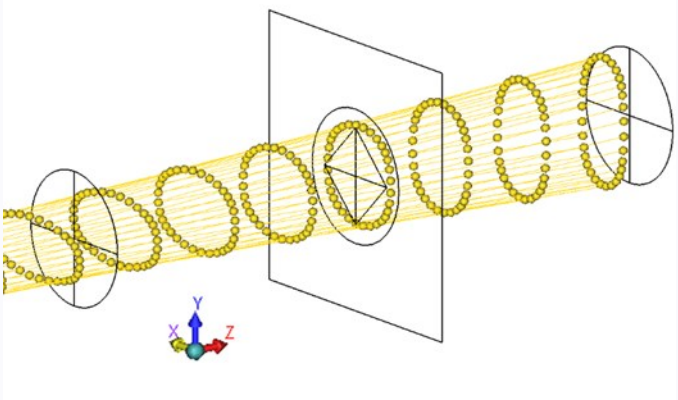

To understand what is happening it is helpful to again consider rays launched from points along the **X** and **Y** axes as shown in the picture below. Here we have only launched two rays from each axis at the endpoints of the emitter surface.

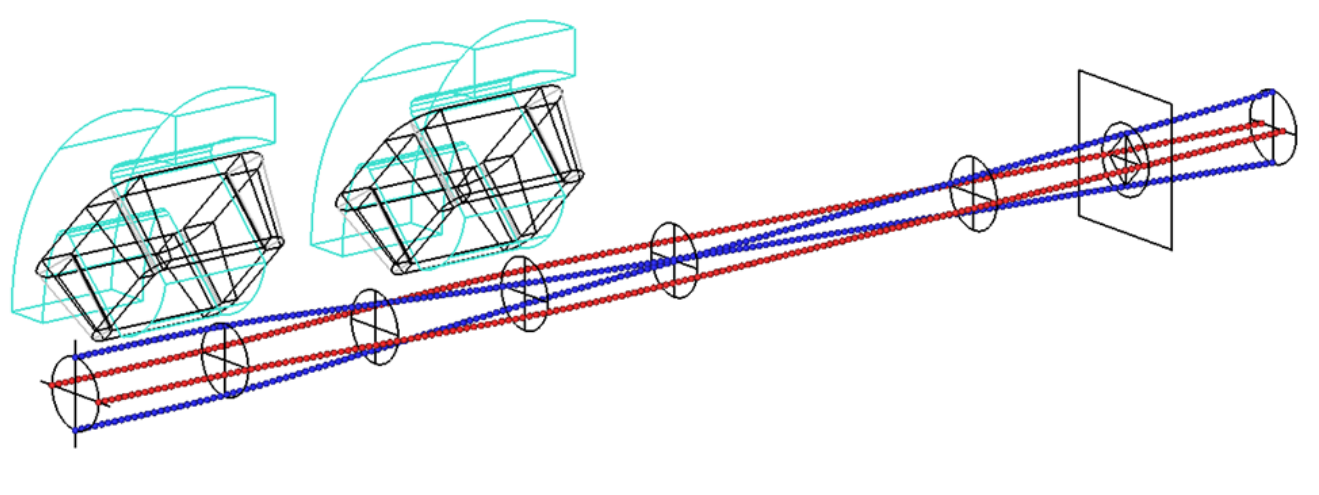

This view provides a clear indication of the first focal point, and the divergence of the blue rays past the focal point. Also it can be seen that although the red rays are converging, the second focal point will be some distance beyond the point of minimum spot size.

At the point of minimum spot size, the divergence of the blue rays and convergence of the red rays is such that the maximum displacement from the beam axis is equal for both. This can be seen in the picture at right. Note that the maximum beam spread and hence spot size is determined by the red rays before the minimum point, and by the blue rays past the minimum point.	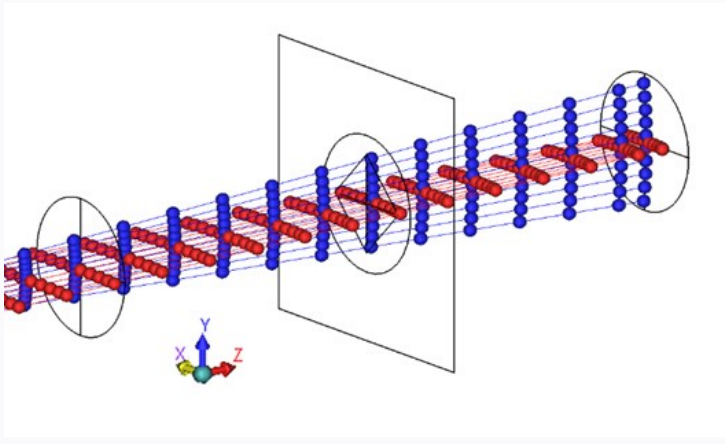

The graph below shows the maximum displacement as a function of distance along the beam axis for both the red and blue rays. At the **Z = 0** both displacements are equal to the radius of the emitter (which is **0.15 m** for our example). Further along the axis, the spot size first increases to a local maximum because of the initial defocusing of the red rays and then begins to decrease as the rays pass through the second quadrupole.

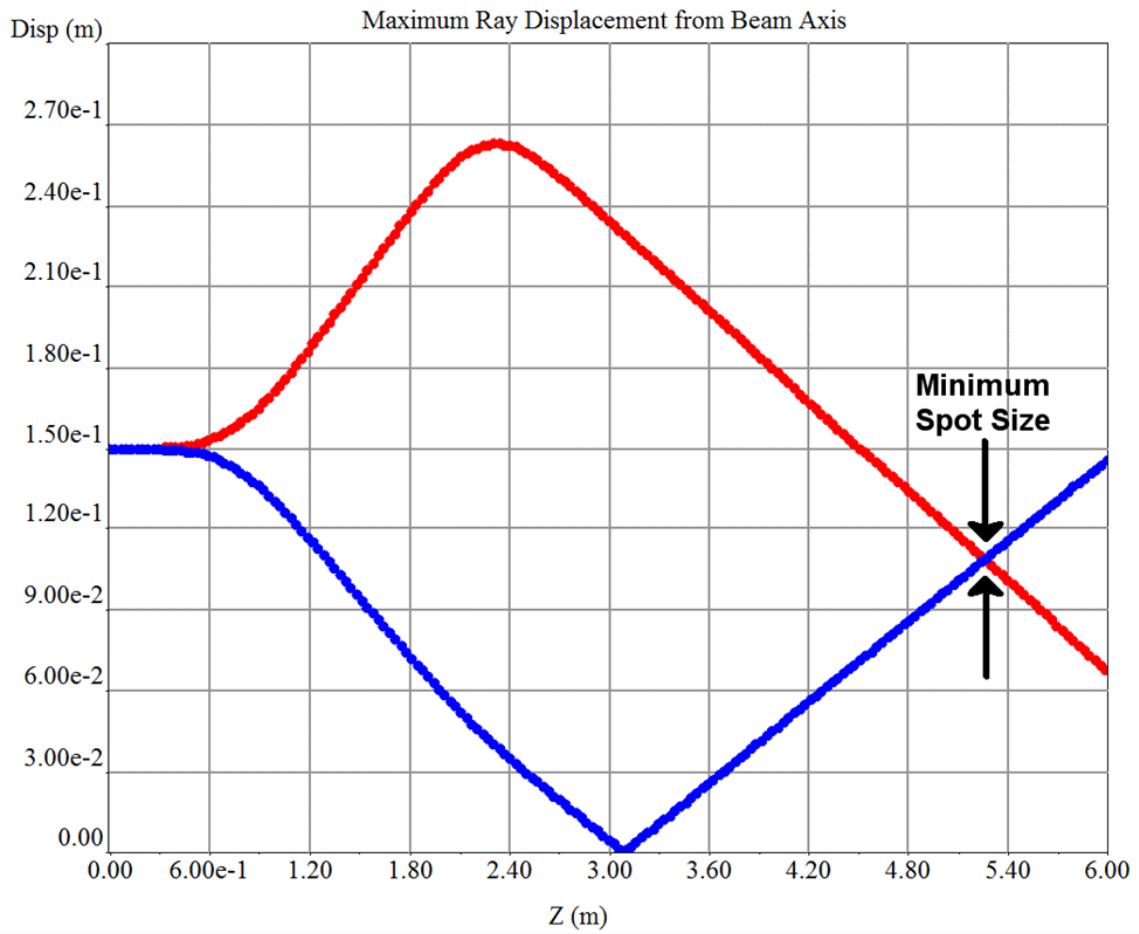

The blue rays converge to a focus and then diverge. At the point of minimum spot size the red and blue rays again have equal displacements. Beyond that the spot size will be determined by the displacement of the blue rays, and it will increase indefinitely until the beam is refocused or terminates at a collector surface.

The local maximum beam spread is of importance since it determines the limits on the maximum level of magnet excitation that can be applied for a given set of particle and energy parameters.

The picture below shows rays launched along the **X** axis which are defocused by the first quadrupole. Arcs have been drawn at the point of maximum spot size to indicate the outlines of the four pole faces.

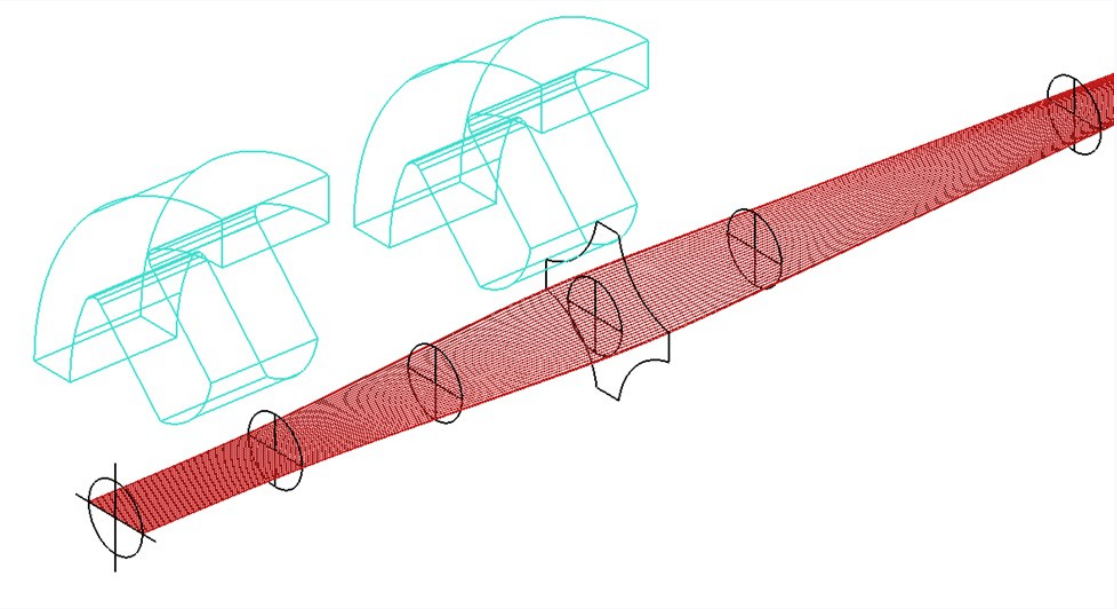

The local maximum beam spread occurs (for our example) just past the middle of the second quadrupole. Past that point, the rays begin to converge.

In the next picture we have reoriented our view and added a circle just large enough to be tangent to the four pole faces. The circle gives a rough indication of the maximum beam spread allowable.	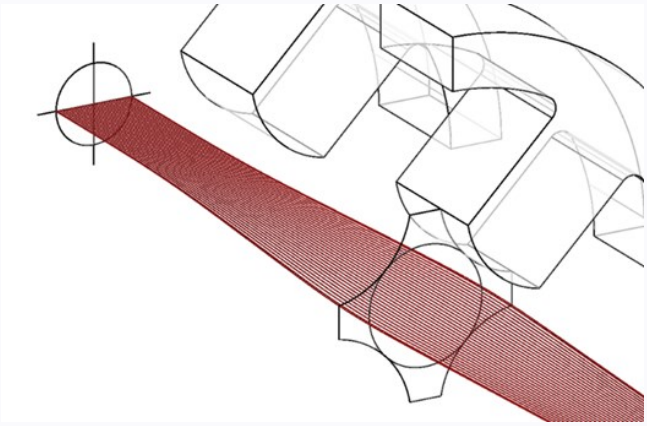

By rotating our view point so that it is more closely aligned with the beam axis, it becomes apparent that at maximum excitation the resulting beam spread will exceed the tangent circle.

A large beam spread is undesirable since it may result in rays which pass outside the region of field uniformity and/or exceed the limits of the vacuum containment chamber.

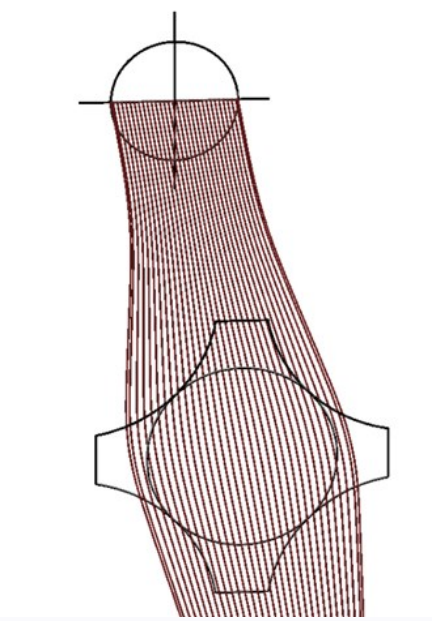

Parametric Variation of Magnet Excitation Level

In the previous section we examined the spot size variation for the case of maximum coil current. In the next sections we will examine the effects of varying the level of excitation using the parametric utility that is a standard feature of **LORENTZ**.

The picture below shows the range of excitation levels we will simulate. The first beam at left shows the results for zero excitation current. Here there is of course no distortion and the beam maintains its initial uniform circular cross section throughout the simulation.

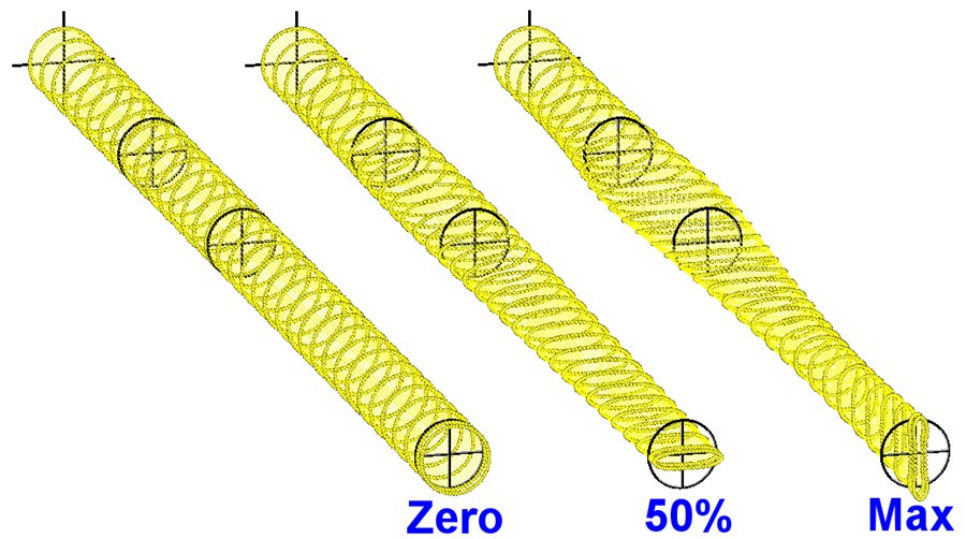

The middle beam shows the effects of **50%** coil current. Here the beam almost reaches the first focus at the end of the simulation. Finally the effects of full excitation are shown for the last beam. By the end of the simulation the beam almost reaches the second focus, and rays that passed through the first focus are diverging.

We will simulate several intermediate levels of excitation. At each level we will have **LORENTZ** calculate the spot size at several points along the beam axis.

Because of the large number of simulation steps and large amount of trajectory data produced, we will present the results in three sections. We will begin with spot size starting at the emitter and ending at the midpoint of the second quadrupole. Then we will examine spot size just beyond the second quadrupole. Finally, we will look at results obtained at some distance beyond the quadrupole pair.

Spot Size Variation for Points from Emitter to Second Quadrupole

In the picture below we have labelled four points along the beam axis from the emitter (center at **Z = 0 m**) to the middle of the second quadrupole (center at **Z = 2.25 m**). As the excitation level is varied the spot size will be calculated on the planes defined by the **Z** coordinates indicated in the picture.

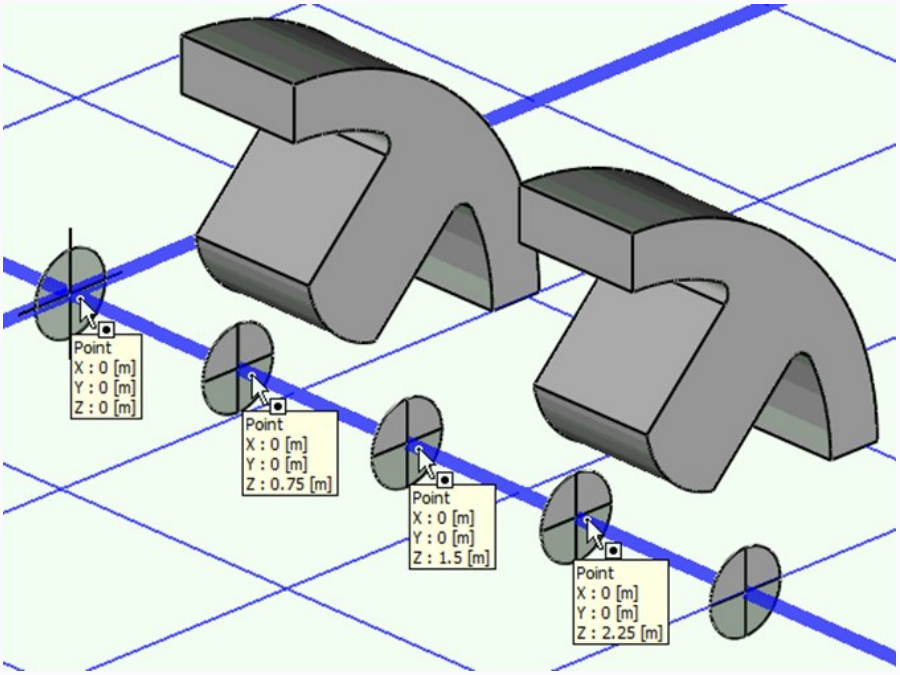

Note that the middle of the first quadrupole is in the plane **Z = 0.75 m**, and the exact midpoint between the two quadrupoles is in the plane **Z = 1.5 m**.

The graphs below shows the variations in spot sizes as excitation level is varied from zero to maximum.

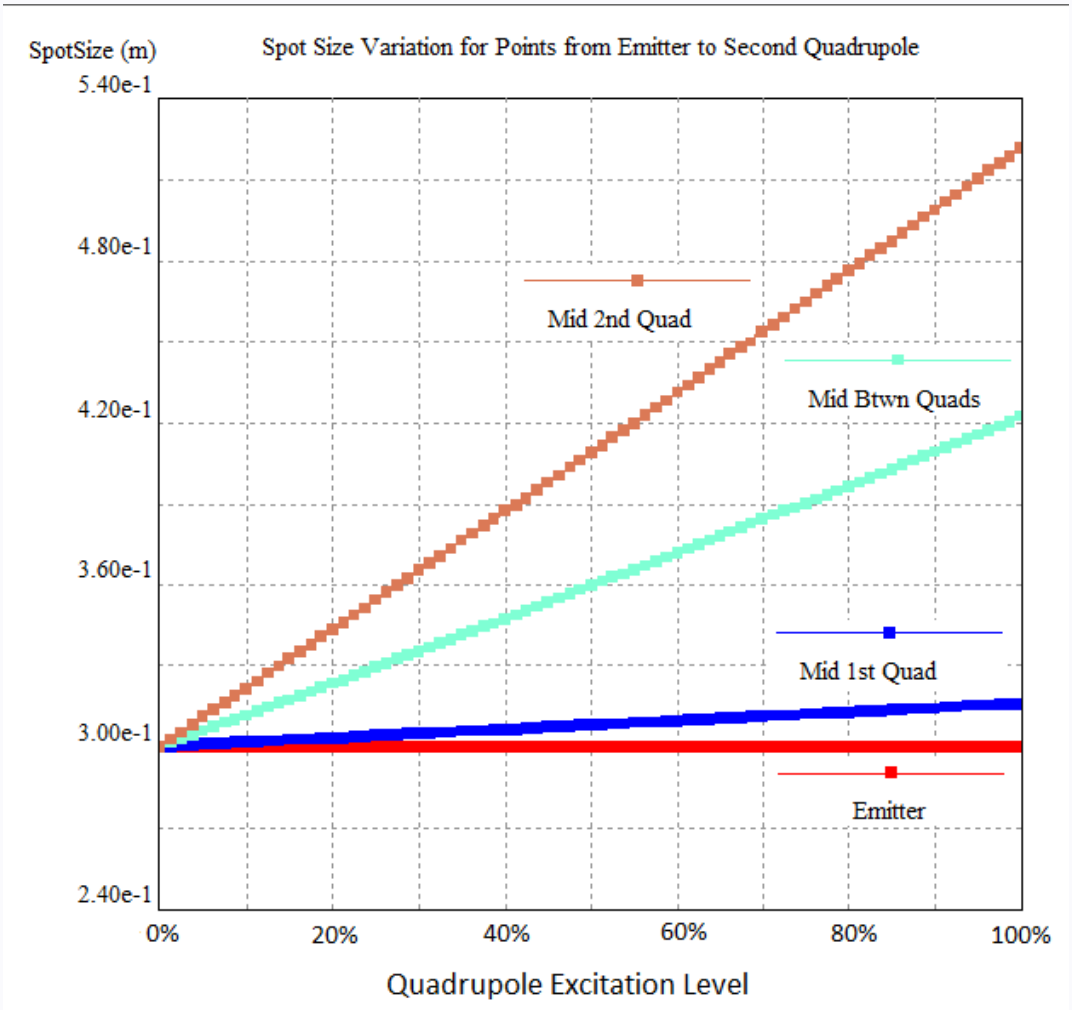

The spot size at the Emitter remains constant which is to be expected. Further along the beam axis the spot size shows an essentially linear increase with increasing excitation levels. Of the four measurement points, the greatest increase in spot size occurs at the very last point which is the middle of the second quadrupole.

These results are consistent with our earlier observation that spot size will be determined by the rays defocused by the first quadrupole until they have traveled far enough along the beam axis to be refocused by the second quadrupole.

Spot Size Variation Beyond Second Quadrupole

In this section we will examine spot size variations for points beyond the second quadrupole. We will consider points at **3**, **4.5** and **6 meters** beyond the emitter as shown in the picture below.

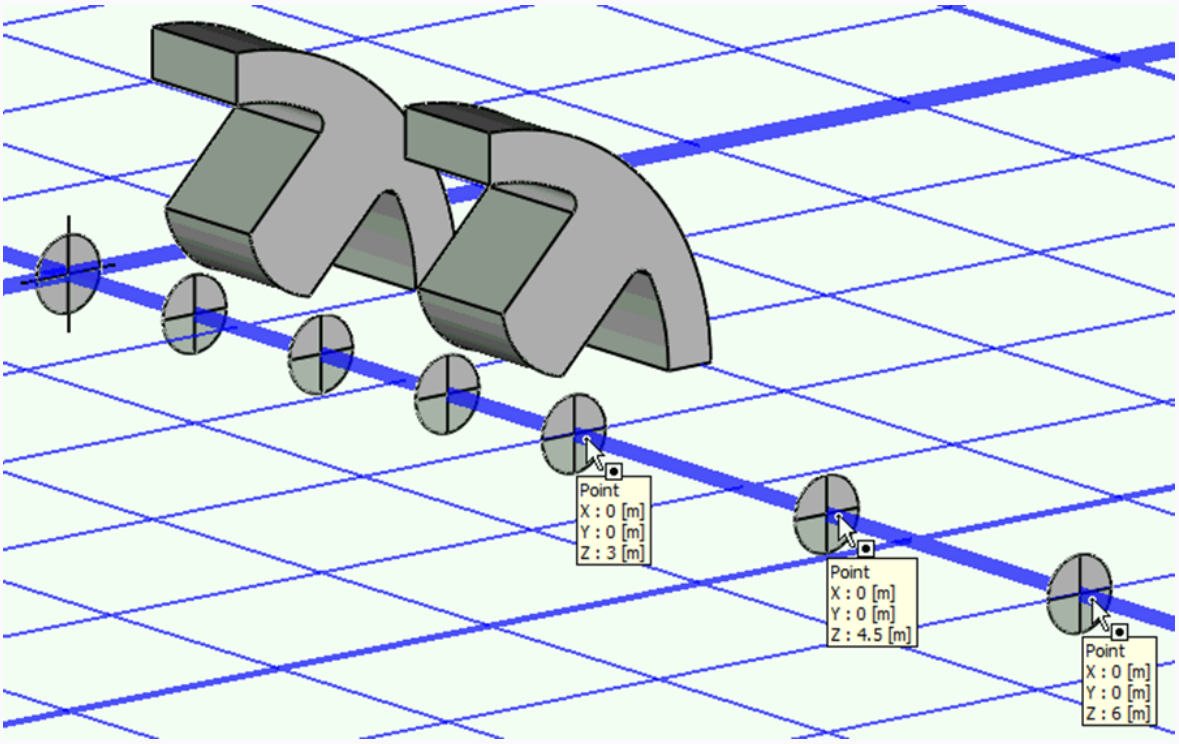

The graphs below shows the variations in spot sizes as excitation level is varied from zero to maximum. Note that at **Z = 3 m** spot size increases with current but the rate of increase slows at higher current levels. At **Z = 4.5 m** the spot size reaches a maximum at about **50%** excitation and then decreases till at full excitation it is about the same as the spot size at the emitter.

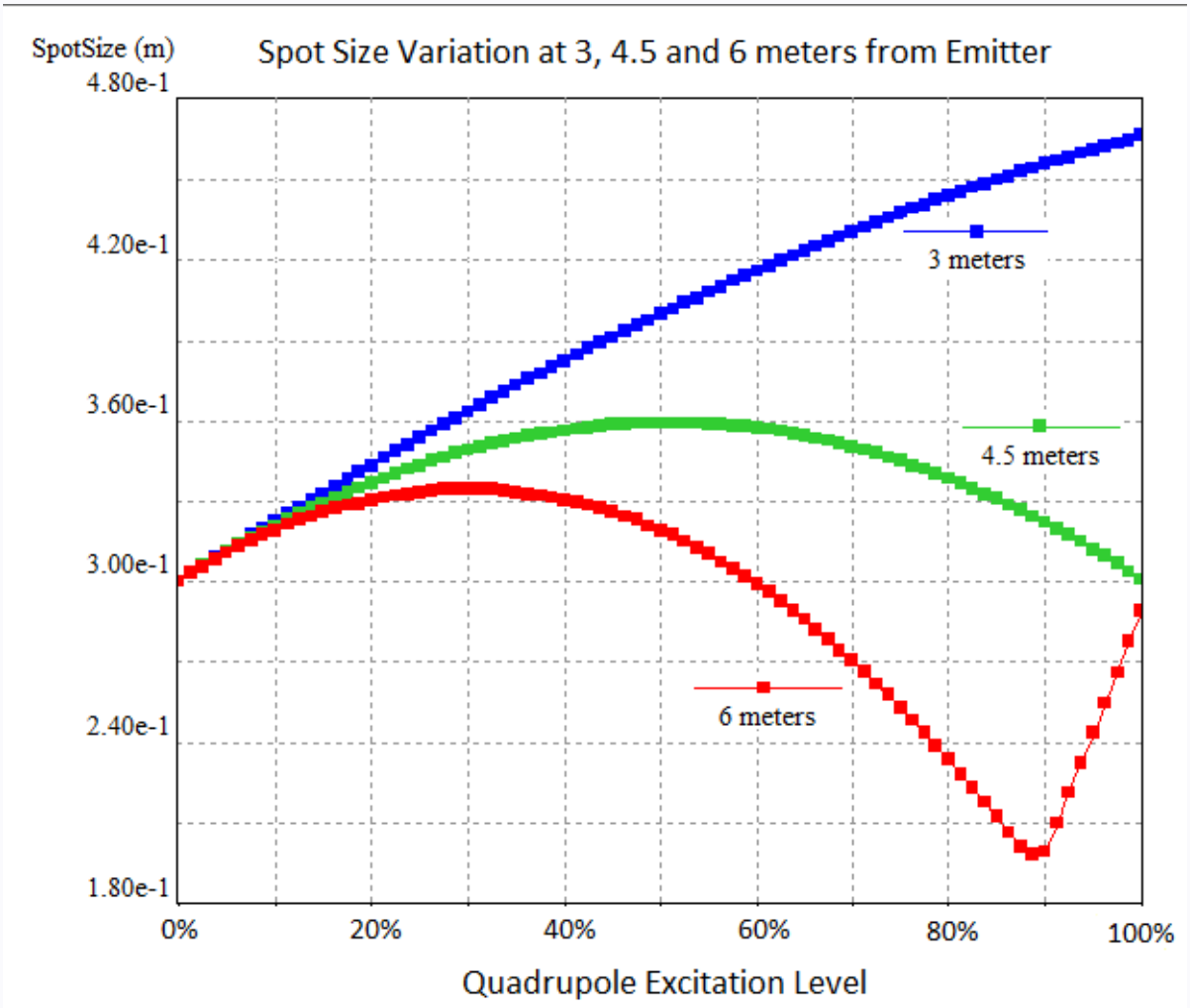

The most interesting behavior occurs at **Z = 6 m**, where the spot size first reaches a maximum at about the **30%** excitation level, and then decreases to a minimum value near the **90%** excitation level. At this minimum, the spot size has been reduced significantly so that it is only about **66%** of the emitter spot size. Further increases of excitation result in an increase of the spot size, so for **Z = 6 m** we can say that **90%** excitation is the optimal level for minimum spot size.

Spot Size Variations at Greater Distances

The graphs below shows the variations in spot sizes as a function of excitation level for distances of **9**, **12** and **15 meters** from the emitter. They demonstrate the same characteristics as were seen previously at **Z = 6 m**.

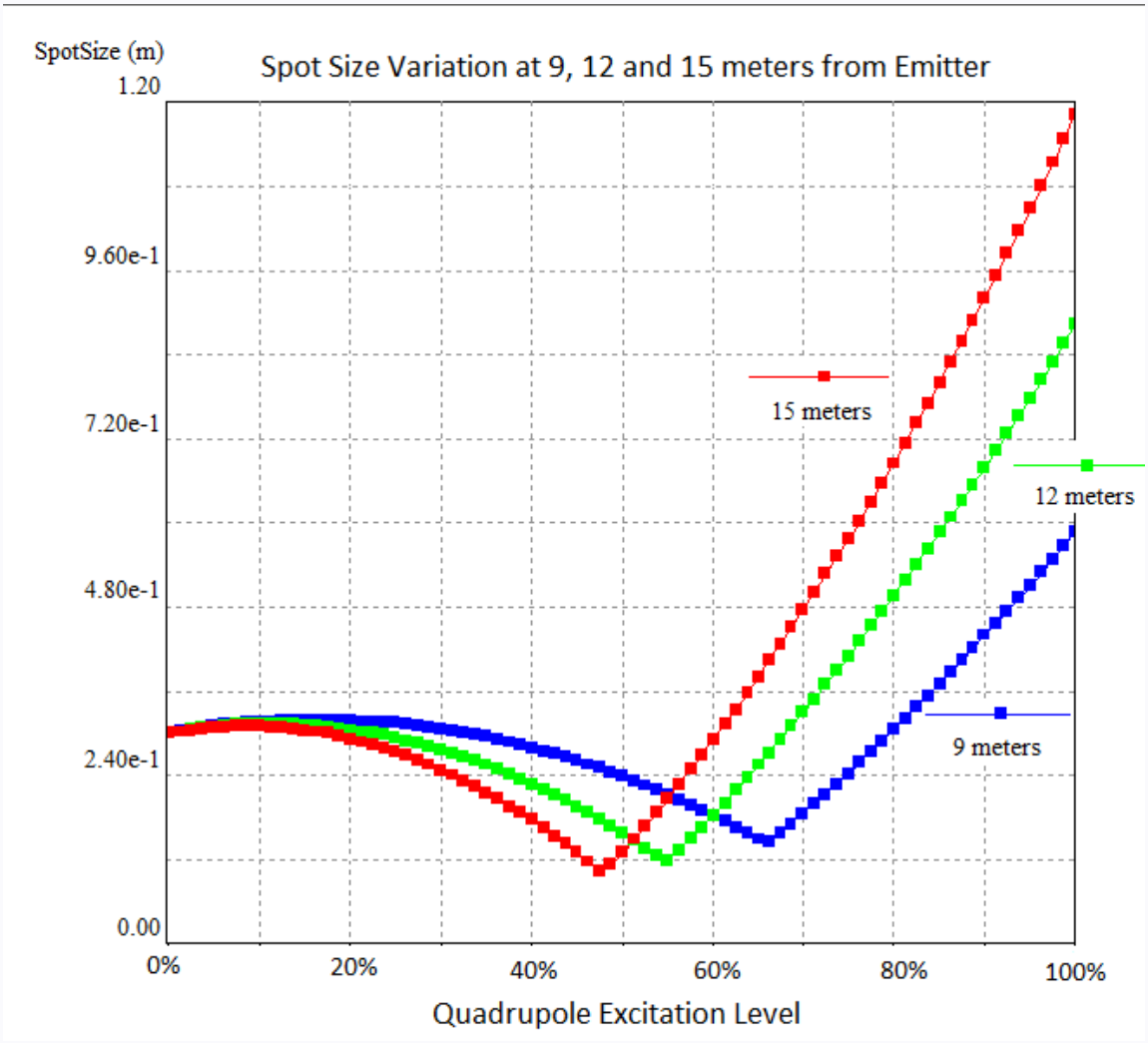

The graphs also show that as distance from the emitter increases, both the minimum spot size and the optimum excitation level decrease.

General Observations on Optimum Spot Sizes

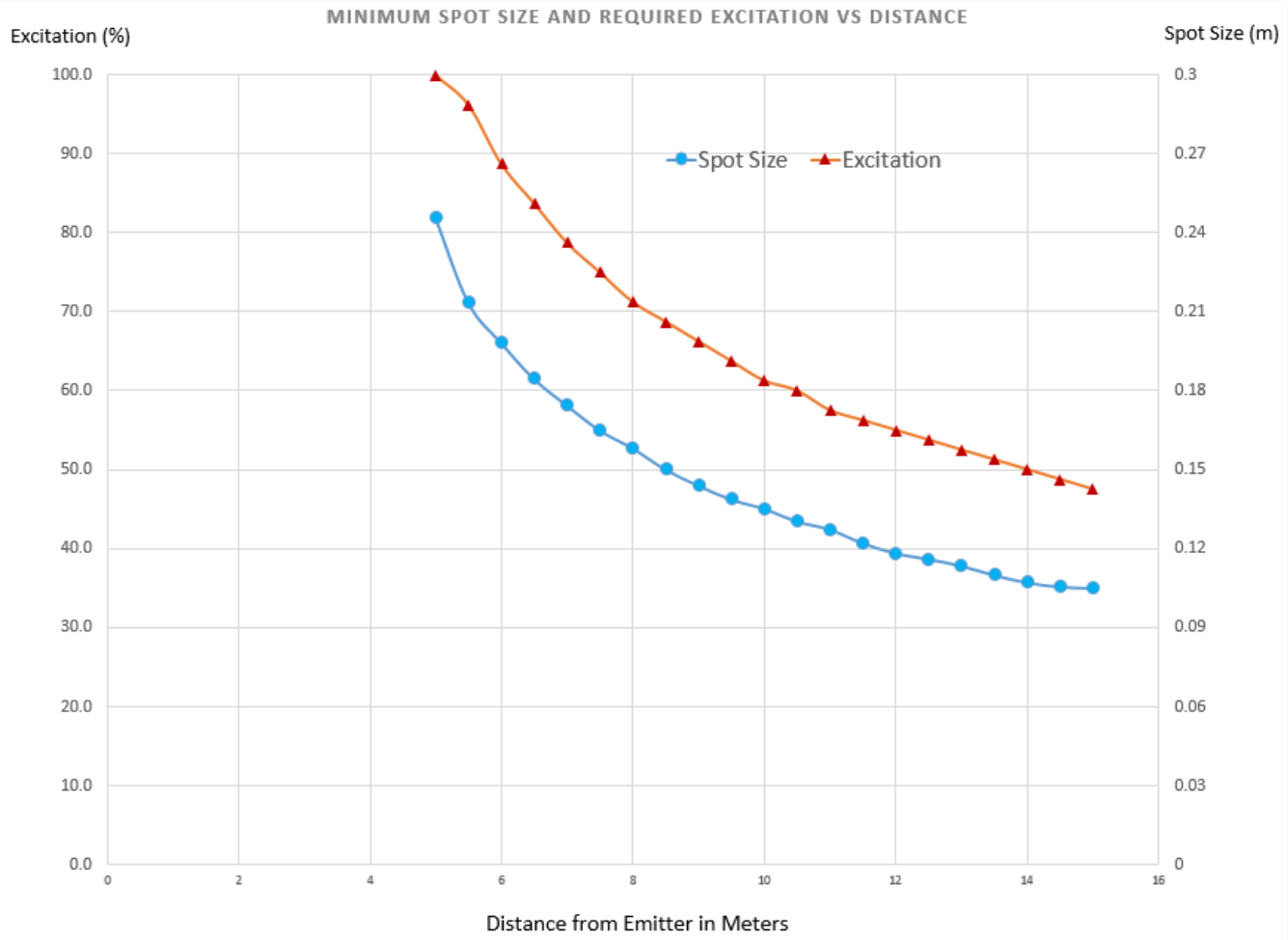

The graphs below summarize the minimum spot sizes and required excitation levels for a range of points from **5** to **15 meters** from the emitter.

To illustrate why this occurs, we have plotted the displacements of the outermost rays under both maximum and **50%** excitation in the graph shown below. Here the thick lines indicate maximum excitation and the thin lines indicate **50%** excitation. We've also drawn rectangles to indicate the locations for minimum spot size.

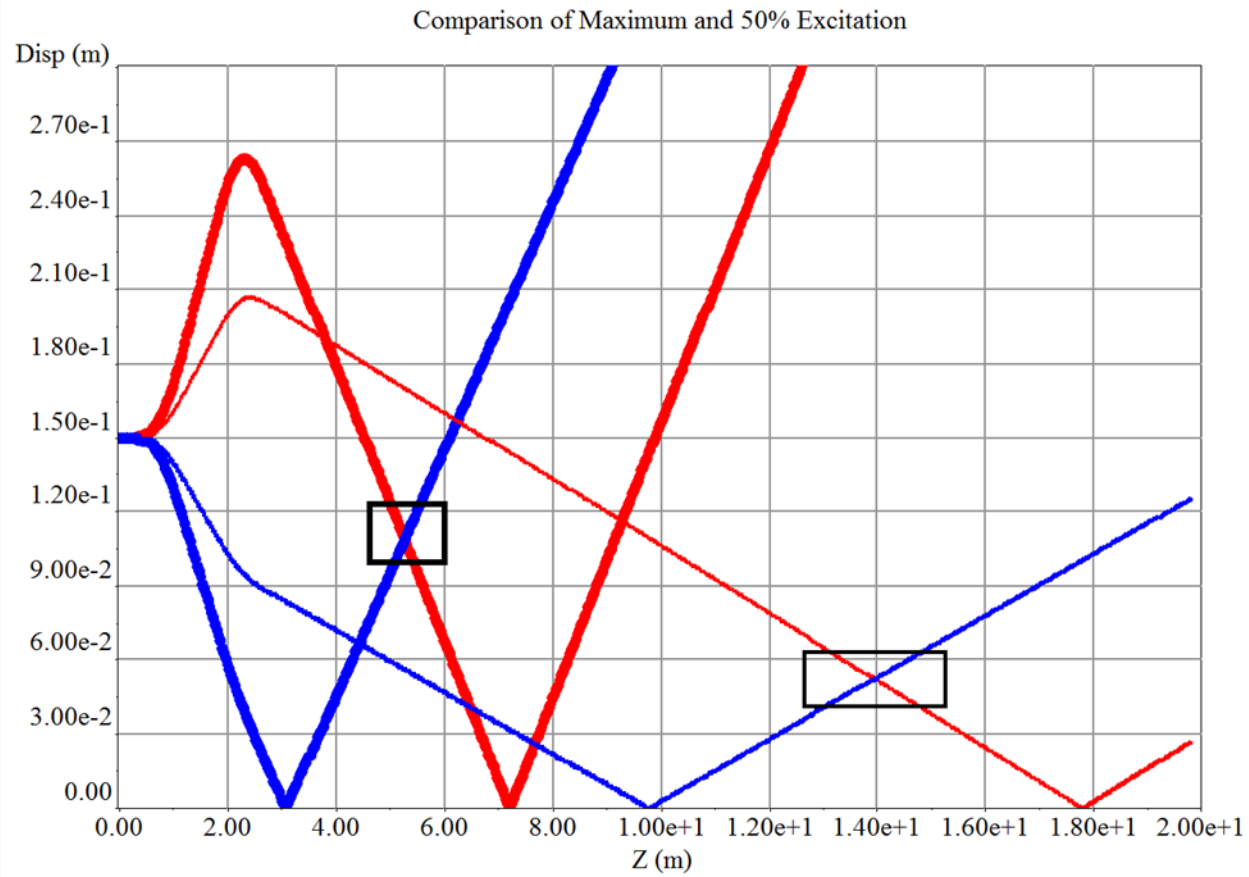

The rays that experience initial defocusing are deflected less for the **50%** excitation. For all rays, the lower excitation level results in both a more gradual convergence to focus and a more gradual divergence after the focal point. The net result is a smaller spot size though at a greater distance along the beam axis.

Summary

Based on the models studied in this paper, we can draw the following conclusions.

- Launching rays from the perimeter of an emitter surface provides a fast efficient method of computing spot size provided that space charge effects are not important.

- Varying magnet excitation parametrically enables the determination of the optimal level for obtaining minimum spot size at points along the beam axis.

- For a given set of beam parameters and quadrupole configuration, the smallest spot sizes can be obtained by allowing the greatest practical amount of beam travel. This will have the additional benefit of requiring lower levels of magnet excitation and hence be more energy efficient as well.

As a final comment, we will note that the parametric utility in **LORENTZ** can easily vary other characteristics of quadrupole models such as spacing between the magnets and the materials and/or dimensions of the magnets themselves. By using nested parametric loops, each model variation can be run through the excitation parametric described in this paper to further increase the possibilities in selecting optimal designs.

About INTEGRATED Engineering Software

Since its inception in 1984, INTEGRATED Engineering Software has created simulation tools that reflect the inspiration of our customers: thousands of engineers and scientists who, everyday, push the boundaries to envision what is possible. They take their ideas from a realm that is almost science fiction and bring them to reality.

As the name of our company suggests, all our programs are seamlessly integrated, starting from a concept, through entry of the geometry and physics of the problem, to the selection of type of solver and the problem's solution. Once the problem has been solved, a vast number of parameters can be calculated or the field quantities displayed.

INTEGRATED Engineering Software is a leading developer of hybrid simulation tools for electromagnetic and particle trajectory analysis. We provide a complete line of fully integrated 2 and 3 dimensional simulation software.

Since the creation of our company, our focus has always been here and our experience has grown hand-by-hand with a great recognition in our market.

INTEGRATED is staffed with leading R&D engineers in areas such as electrical engineering, magnetics, and high frequency applications. Our tools are used in a wide variety of industries, including manufacturing, automotive, medical, telecommunications, power, health care and aerospace markets, as well as universities and research laboratories.

INTEGRATED products allow engineers and scientists to reduce design cycles, save time and money and deliver more efficient products to the market faster than ever before.

INTEGRATED empowers engineers and scientists with many options to choose from:
The best solvers for each specific application: Boundary Element Method (BEM), Finite Element Method (FEM) or Finite Difference Time Domain (FDTD) solvers. The best optimization tool for each particular design: parametric analysis, scripting or application programming interface (API)

INTEGRATED's commitment is to provide designers with the most sophisticated analysis tools to assist them in the creation of the future.

Contact us for an evaluation

Send us your model, whatever the level of complexity. **We will show you how to get results from your exact design** – no packaged demos.

Contact us for an evaluation and start improving productivity today. A live demo is also available.

Phone: +1 204 632 5636
Fax: +1 204 633 7780
Email: info@integratedsoft.com
Website: www.integratedsoft.com

INTEGRATED
ENGINEERING SOFTWARE